Available online at www.sciencedirect.com
ScienceDirect
Journal of Electroanalytical Chemistry 614 (2008) 49–60
Journal of Electroanalytical Chemistry
www.elsevier.com/locate/jelechem

Capacitance, spectroelectrochemistry and conductivity of polarons and bipolarons in a polydicarbazole based conducting polymer

Zvika Pomerantz [a], Arie Zaban [a], Subrata Ghosh [a], Jean-Paul Lellouche [a], Germà Garcia-Belmonte [b], Juan Bisquert [b,*]

[a] Department of Chemistry, Bar-Ilan University, Raman-Gan 52900, Israel
[b] Departament de Física, Universitat Jaume I, 12071 Castelló, Spain

Received 10 August 2007; received in revised form 5 November 2007; accepted 8 November 2007
Available online 21 November 2007

Abstract

The paper discusses the interpretation of electrochemical and spectroelectrochemical measurement of charging and transport of electronic species in conducting polymers, as a function of the polymer potential. The charging is accessible via two independent methods of measuring the chemical capacitance, C_μ: electrically, by cyclic voltammetry (CV), and optically, by the light absorption. The conductivity, σ, is measured by the microband electrode method. We formulate the models of the chemical capacitance for the formation of polarons and bipolarons in the presence of Gaussian disorder in the energy levels. This gives rise to the appearance of either one or two broad peaks in CV, depending on the formation energies of the polaron and bipolaron species. We also discuss the interpretation of the diffusion coefficient D_p and conductivity in the presence of a broad disorder. We find that the relation $\sigma = C_\mu D_p$ is generally valid, and application of the generalized Einstein relation allows us to find also the properties of the carrier mobility, u_p. A decrease of the mobility at very high carrier densities is expected because the density of states (DOS) is finite, and the transport is limited by the decrease of available empty transport sites. The observation of separate capacitance peaks for polarons and bipolarons is reported in a polydicarbazole based conducting polymer, namely poly[2,6-bis-carbazole-9-yl-hexanoic acid pentafluorophenol ester]. The measured conductivity displays the expected feature, on the basis of the model, of a decrease when the DOS is saturated at high oxidation levels.

Keywords: Conducting polymers; Hopping transport; Capacitance; Voltammetry

1. Introduction

Conjugated polymers are actively investigated for applications such as optoelectronic devices, organic electronics and sensors. A number of methods have been used to address the nature of charge carriers induced by electrochemical doping and the associated changes in the polymer during oxidation–reduction: Cyclic voltammetry (CV) [1,2], electrochemical impedance spectroscopy (EIS) [3,4], in situ conductivity [5], EPR and spectroelectrochemistry [6]. However, the interpretation of such measurements raises several issues that are yet not completely understood.

When a conducting polymer is oxidized electrochemically, the holes in the polymer chains are self-trapped by the local polarization, creating polarons (P) which can move only by carrying along the associated structural deformation. Two polarons in a single polymer chain can form a bipolaron (B), since the energy gained by forming only one deformation may outweight the increased Coulomb repulsion energy. The dependence of the P and B densities on the electrochemical potential during oxidation of conducting polymers can be described by a well known model based on equilibrium among the neutral, P and B states [1,6–8]. This model amounts to the statistics of non-interacting carriers allowing for both single and double occupation of sites in the lattice of localized sites [9]. The nature of the charge carriers at high doping levels

* Corresponding author.
E-mail address: bisquert@fca.uji.es (J. Bisquert).

0022-0728/$ - see front matter © 2007 Elsevier B.V. All rights reserved.
doi:10.1016/j.jelechem.2007.11.005

has been debated, and it was pointed out [10] that π dimers are a likely alternative to bipolarons in highly doped conducting polymers, but here we base our analysis on the simple P–B model [8,10]. It is generally observed that the CV of electronically conducting polymers is characterized by broad non-Nernstian waves and a theory previously presented [11], directly related the broad shape of CV peaks usually found to the Gaussian density of states (DOS) that is characteristic of disordered organic conductors [12,13]. The relationship was confirmed in the interpretation of CV peaks of polypyrrole [11] and the hole conductor spiro-OMeTAD (2,2′7,7′-tetrakis(*N*,*N*′-di-*p*-methoxyphenyl-amine)-9,9-spiro-bifluorene) [14], see also the review paper [15]. However, in these reports [11,14] a single CV peak was observed. So far a conclusive interpretation of separate P and B peaks using this model has not been made, and this will be shown below, by combining CV and spectroelectrochemistry measurements.

Since many of the applications of the conducting polymers (light emitting diodes, lightweight batteries, etc.) involve charge transport, the mechanisms governing the electronic conductivity in these materials as a function of the degree of doping are of outmost interest. Hole transport is measured electrochemically by bridging a microband electrode with the polymer [5]. The hole conductivity is given by

$$\sigma = epu_{\mathrm{p}} \tag{1}$$

where e is the elementary positive charge, p is the total hole density and u_{p} is the hole mobility. Over the years, an increasing amount of evidence shows a general pattern for the conductivity and mobility as a function of electrochemical doping [5,16–27]. At increasing oxidation levels, σ shows a large increase, then a saturation and decrease at the more positive potentials [5,16–25], see Fig. 9d below. Early reports [16,17] found that the conductivity σ follows the shape of the CV, and also that the region of high conductivity is a restricted window of oxidation potentials. In addition, the mobility also shows a remarkable variation on oxidation potential. At low to moderate doping levels u_{p} exhibits a constant (or decreasing) region, while at high oxidation levels, it first increases steeply, sometimes over several orders of magnitude, and later decreases [23,28]. While the increase of the conductivity is a normal consequence of the increasing levels of carrier density (p) by electrochemical doping, the decrease at very high carrier densities has received different explanations. Sometimes the decrease of σ has been attributed to the degradation of the polymer [23], while in other cases such effect has been clearly discarded [20], since the maximum of σ was recovered in an reduction scan. The decrease of conductivity has also been attributed to structural modifications [18,24].

In general, charge carrier transport in molecular and organic materials is dominated by charge localization resulting from polarization of the medium and relaxation of molecular ions. As a result of weak intermolecular interactions, the carriers in these materials are strongly localized on a molecule, and transport occurs via a sequence of charge-transfer steps from one molecule to another [29]. The low mobility of the charge transport in polymers is mainly due to the obstacle for carriers to travel to jump over a neighboring chain. Even if the polymer chains are well-ordered, macroscopic transport is impossible unless the carrier can hop to avoid the chain break and defects [30]. One of the objectives of the present work is to clarify the meaning of the transport coefficients (mobility, diffusion coefficient) measured by electrochemical methods in such complex situations. It is important to remark that experimental results on quasi-equilibrium CV and carrier transport in conducting polymers, are strongly influenced by the shape of the DOS, so both features have to be treated combinedly. In particular, our theoretical framework quite naturally incorporates the idea that the saturation of the DOS at high carrier densities prevents long range transport of carriers, which was enunciated in some papers [16,17,20] as the origin of the leveling and decrease of the conductivity at high oxidation potentials.

In this paper, we discuss the electrochemical behavior of a polydicarbazole based conducting polymer (di-Cbz-PFP), namely poly[2,6-bis-carbazole-9-yl-hexanoic acid pentafluorophenol ester]. The syntheses of the monomer (Fig. 1) as well as detailed analysis of the polymerization process was reported [31]. It was found that the polymer insulator to conductor transition is highly affected by the nature of the group on the chiral center [31,32]. In the case of di-cbz-PFP, the oxidation potential of the PFP neighboring carbazole (Cbz a in Fig. 1) was shown to shift positively as a result of the highly electron attracting nature of the PFP group. Consequently polymer charging and the following processes, like polarons–bipolaron transitions (elaborated below), spread over a wide potential window. We note that in previous publications [31,32] we relate the high potential broad peak to oxidation of dangling bonds, i.e. carbazole units that are not part of the polymer backbone. However, new experimental data lead us to the understanding that this broad peak relates solely to the formation of bipolarons. Full analysis based on this concept will be published in the near future. In brief, we found that the broad high potential peak in the CV presents classic spectral behavior of bipolaron as will be discussed later on. Moreover, the basic shape of the CV did not change

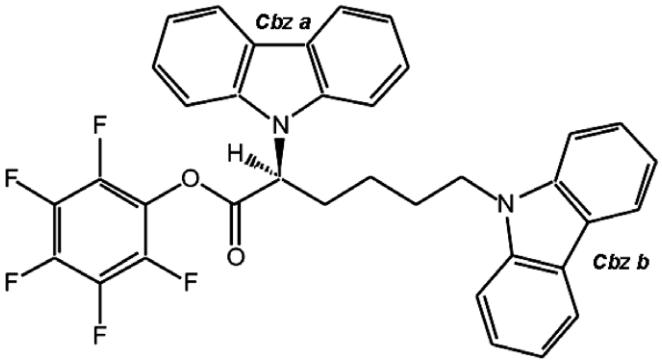

Fig. 1. Chemical structure of the monomer used in this study.

by forced increase of the dangling units density of the polymer. Finally, chemical manipulation of the polymer to remove the PFP units shows correlation between the width of the high potential peak and the bipolaron spectroscopy.

The structure of the paper is as follows. In Section 2 we discuss the theoretical concepts for analyzing the electrochemical data in terms of the energy disorder. This allows us to describe the capacitance of P and B species as a function of the electrochemical potential. The properties of the conductivity and transport coefficients (diffusion coefficient, mobility), are discussed theoretically in Section 3. Section 4 describes the experimental procedures, and Section 5 is an analysis of the experimental results in terms of the model outlined in Sections 2 and 3.

2. Equilibrium statistics and chemical capacitance

Here, we outline briefly the model of Ref. [11] for the analysis of CV peaks, to facilitate the interpretation of the experimental results presented below. The polymer is considered as a collection of N_s conjugated chain segments per unit volume, each containing m monomers. These segments describe the extension of polarons or bipolarons in the polymer chain, so that each segment contains at most one charged excitation (P or B). Taking the energy reference at the center of the gap of width 2ε, the energy for adding an electron is $\varepsilon_c = \varepsilon$, and the energy for extracting an electron (adding a hole to the valence band) is $\varepsilon_v = -\varepsilon$. When a hole is added to the polymer, relaxation of the atomic positions will occur extremely rapidly. The energy of the P formation, $-\varepsilon_P$, is lower than that of the unrelaxed hole, ε_v. Further, the total energy of formation of a double charged excitation (B) is $-\varepsilon_B$ [8,33].

Let p be the total density of holes in the form of polarons and bipolarons, $E_F(p)$ the electrochemical potential of holes, or Fermi level ($\eta = E_F$), and $\mu(p)$ the chemical potential. Note that

$$E_F = e\phi + \mu \tag{2}$$

where ϕ is the local electrostatic potential. In quasiequilibrium conditions, a change of the electrode potential modifies the Fermi level as $e\mathrm{d}V = \mathrm{d}E_F = \mathrm{d}\mu$. The chemical capacitance (per unit volume) is defined as [11]

$$C_\mu = e^2 \frac{\mathrm{d}p}{\mathrm{d}\mu} \tag{3}$$

and it is related to the current per unit area in cyclic voltammetry (CV), j, as [11]

$$C_\mu = \frac{j}{sL} \tag{4}$$

where s is the scan rate and L is the film thickness. In the zero-temperature limit, the capacitance is related to the DOS function as [34]

$$C_\mu = e^2 g(E_F) \tag{5}$$

This last approximation has a limited validity at low carrier densities in a Gaussian DOS, as discussed later in Fig. 3b.

Assuming first that only single occupancy (P) of the localized sites is possible, all with unique energy ε_P, the carrier density is given by

$$p = N_s f_P(E_F, \varepsilon_P) \tag{6}$$

Here f_P is the Fermi-Dirac function

$$f_P(E_F, \varepsilon_P) = \frac{1}{1 + e^{(\varepsilon_P - E_F)/k_B T}} \tag{7}$$

where k_B is Boltzmann's constant and T is the temperature. The chemical capacitance of polarons has the value

$$C_\mu = \frac{N_s e^2}{k_B T} f_P(1 - f_P) \tag{8}$$

This is the standard form of the "redox capacitance" for a nernstian species [35]. It forms a peak at the standard potential ($f_P(\eta_0, \varepsilon_P) = 1/2$), with a slope of 60 mV/decade at the cathodic side. The carrier density and chemical capacitance dependence on Fermi level are shown in Fig. 2a. Note that Eq. (7) is equivalent to the Langmuir isotherm and takes also the form

$$E_F = \varepsilon_P + k_B T \ln \frac{p}{N_s - p} \tag{9}$$

The energy disorder that is characteristic of organic conductors usually has the form of a Gaussian function [15,36]

$$g(\varepsilon) = \frac{N_s}{\sqrt{2\pi}\sigma_P} \exp\left[-\frac{(\varepsilon - \varepsilon_P)^2}{2\sigma_P^2}\right] \tag{10}$$

The carrier density is found as

$$p = \int_{-\infty}^{+\infty} g(\varepsilon) f_P(E_F, \varepsilon)\mathrm{d}\varepsilon \tag{11}$$

and chemical capacitance is

$$C_\mu = e^2 \int_{-\infty}^{+\infty} g(\varepsilon) \frac{\mathrm{d}f}{\mathrm{d}E_F}(E_F, \varepsilon)\mathrm{d}\varepsilon = \frac{e^2}{k_B T} \int_{-\infty}^{+\infty} g(\varepsilon) f(E_F, \varepsilon)[1 - f(E_F, \varepsilon)]\mathrm{d}\varepsilon \tag{12}$$

Fig. 3a and b show the charging properties of the Gaussian DOS. In Fig. 3b it is observed that high (>10%) charging level, the capacitance reflects the shape of the DOS and displays a parabolic form in semilog representation. This is expected in the standard approximation, Eq. (5), used in charging experiments to determine the DOS [13]. However, at occupation level <1% the chemical capacitance diverges from this approximation. This is because of the features of the Gaussian DOS. At very low charging densities, the carriers agglomerate at the tail of the Gaussian distribution. The mean energy of the carriers is independent of the Fermi level, and has the value $E_m = \sigma_P^2/k_B T$, indicated in Fig. 3a. For $E_F < E_m$, most of the hole carriers are symmetrically distributed around E_m and are, therefore, situated between the Fermi level and the center of the DOS

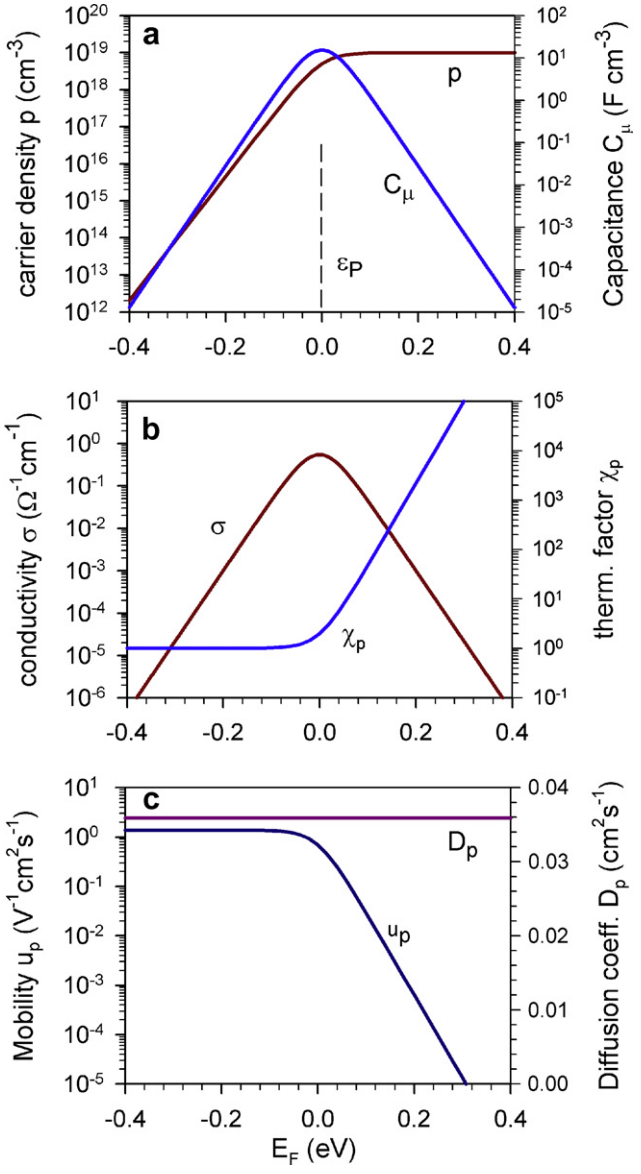

Fig. 2. Representation of several quantities for carrier accumulation and transport by hopping between localized states in a material with a single level of energy $\varepsilon_p = 0$ eV. E_F is the Fermi level potential. (a) Carrier density and chemical capacitance. (b) Conductivity. (c) Mobility and chemical diffusion coefficient. The following set of parameters was used in the calculation: $N_s = 1.0 \times 10^{19}$ cm^{-3}, $T = 300$ K, $v_0 = 10^{12}$ s^{-1}.

[37,38]. Therefore, in the Gaussian DOS at $E_F < E_m$ the Boltzmann approximation can be used in Eq. (11). The carrier density is given by

$$p = \int_{-\infty}^{+\infty} g(\varepsilon) \exp\left(-\frac{\varepsilon - E_F}{k_B T}\right) d\varepsilon = N_s \exp\left(\frac{E_F}{k_B T} - \frac{E_m}{2k_B T}\right) \quad (13)$$

and the chemical capacitance has the value

$$C_\mu = \frac{e^2 N_s}{k_B T} \exp\left(\frac{E_F}{k_B T} - \frac{E_m}{2k_B T}\right) \quad (14)$$

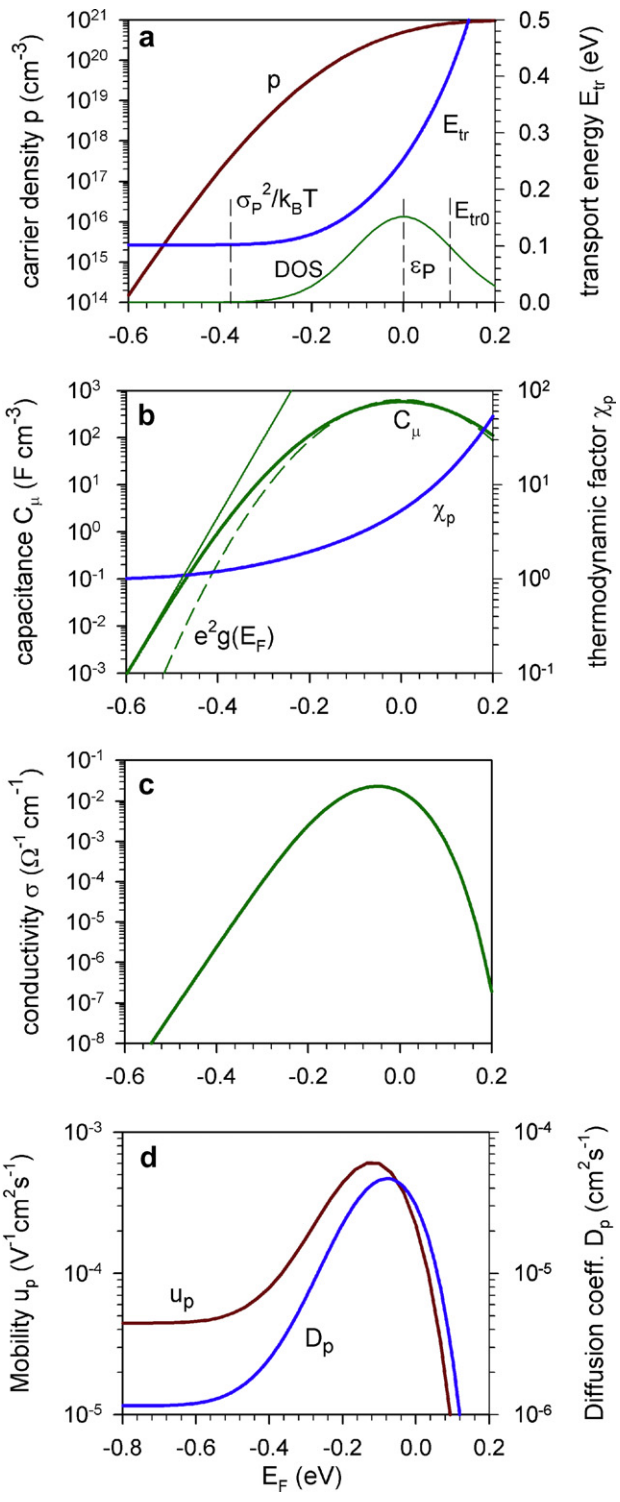

Fig. 3. Representation of several quantities for charge accumulation and transport by hopping between localized states in a material with a Gaussian DOS, according to the transport energy concept. E_F is the Fermi level potential. (a) Carrier density and transport energy. The Gaussian DOS is also shown in linear scale. (b) Capacitance and thermodynamic factor. The thin dashed line is the capacitance according to the approximation $C_\mu = e^2 g(-E_F)$. The thin line is the low density approximation of Eq. (14). (c) Conductivity. (d) Mobility and chemical diffusion coefficient. The following set of parameters was used in the calculation: $N_s = 1.0 \times 10^{21}$ cm^{-3}, $\varepsilon_p = 0$ eV, $\sigma_P = 0.1$ eV, $T = 300$ K, $v_0 = 10^{13}$ s^{-1}, $a = 2 \times 10^{-8}$ cm.

At low charging level the chemical capacitance (that is the quantity determined in step charging experiments) does not reflect at all the shape of the Gaussian DOS, but instead shows an exponential dependence on potential, as shown in Fig. 3b.

The case in which both P and B can be formed upon oxidation, corresponds to equilibrium ratios of the reactions $A \leftrightarrow P^+ + e^-$ and $P^+ \leftrightarrow B^{++} + e^-$ where A is a neutral segment, with density $n_0 = N_s - n_P - n_B$. The distribution functions are [11]

$$f_P(E_F, \varepsilon_P, \varepsilon_B) = \frac{1}{1 + e^{(\varepsilon_P - E_F)/k_B T} + e^{-(\varepsilon_B - \varepsilon_B - E_F)/k_B T}} \quad (15)$$

$$f_B(E_F, \varepsilon_P, \varepsilon_B) = \frac{1}{1 + e^{2(\varepsilon_B/2 - E_F)/k_B T} + e^{(\varepsilon_B - \varepsilon_B - E_F)/k_B T}} \quad (16)$$

The densities of P and B are given by

$$n_P = N_s f_P(E_F, \varepsilon_P, \varepsilon_B), \quad n_B = N_s f_B(E_F, \varepsilon_P, \varepsilon_B) \quad (17)$$

If we describe the distribution of each species with its own characteristic energy and width, the density of states becomes

$$g(E, E') = \frac{N_s}{2\pi\sigma_P\sigma_B} \exp\left[-\frac{(E - \varepsilon_P)^2}{2\sigma_P^2} - \frac{(E' - \varepsilon_B)^2}{2\sigma_B^2}\right] \quad (18)$$

The number of P and B are given by the expressions

$$n_P = \int_{-\infty}^{+\infty} g(\varepsilon, \varepsilon') f_P(E_F, \varepsilon, \varepsilon') d\varepsilon\, d\varepsilon' \quad (19)$$

$$n_B = \int_{-\infty}^{+\infty} g(\varepsilon, \varepsilon') f_B(E_F, \varepsilon, \varepsilon') d\varepsilon\, d\varepsilon' \quad (20)$$

The chemical capacitances take the forms [11]

$$C_\mu^P = e^2 \int_{-\infty}^{+\infty} g(E, E') \frac{df_P}{dE_F}(E_F, E, E') dE\, dE' \quad (21)$$

$$C_\mu^B = 2e^2 \int_{-\infty}^{+\infty} g(E, E') \frac{df_B}{dE_F}(E_F, E, E') dE\, dE' \quad (22)$$

The features of carrier density and chemical capacitance in the above Gaussian disorder model for both P and B are illustrated in Figs. 4 and 5. First, Fig. 4 shows a situation in which the formation of a B is energetically favored over two Ps, i.e. $2\varepsilon_P > \varepsilon_B$. At low oxidation levels only Ps are formed, since the single carriers are scarce and cannot aggregate, but when the electrochemical potential approaches the value $\varepsilon_B/2$, the recombination of Ps into Bs occurs and Bs dominate the carrier distribution, Fig. 4a. Consequently the CV mainly shows a unique peak of Bs, Fig. 4b, with the peak broadness being determined by the energy spread of the DOS, σ_B, see Eq. (5). Interestingly, the capacitance of Ps displays a negative contribution, because their number decreases while the electrochemical potential (i.e. the thermodynamic driving force for formation) increases.

The opposite case, in which the formation of P is energetically favored ($2\varepsilon_P < \varepsilon_B$) is shown in Fig. 5. Now the formation of Bs is delayed in comparison with the former example, but nonetheless it finally takes place. It is driven by the entropic force associated with larger concentration

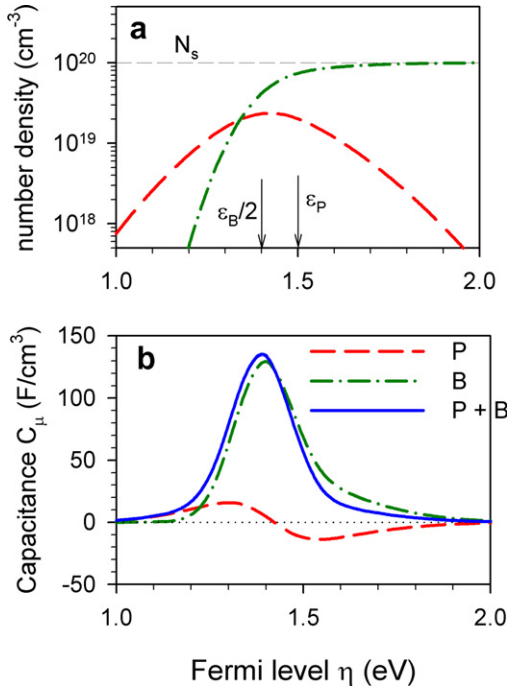

Fig. 4. Simulation of the electrochemical charging for a polymer with site density $N_s = 10^{20}$ cm^{-3}. The polaron levels are centered at $\varepsilon_P = 1.5$ eV with dispersion $\sigma_P = 0.2$ eV, and the bipolaron levels are centered at $\varepsilon_B = 2.8$ eV with dispersion $\sigma_B = 0.15$ eV. (a) Number density of polarons and bipolarons. (b) Chemical capacitance of polarons, C_μ^P, bipolarons, C_μ^B, and total capacitance, as a function of Fermi level.

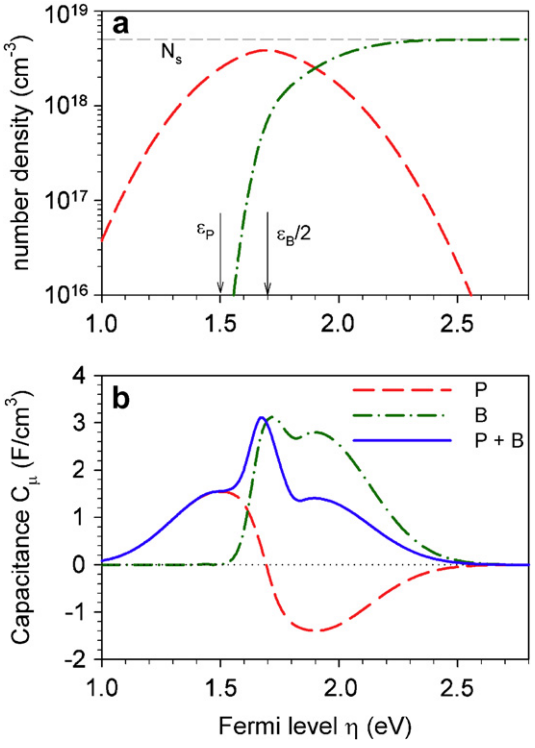

Fig. 5. Simulation of the electrochemical charging for a polymer with $N_s = 5 \times 10^{19}$ cm^{-3}. The polaron levels are centered at $\varepsilon_P = 1.5$ eV with dispersion $\sigma_P = 0.2$ eV, and the bipolaron levels are centered at $\varepsilon_B = 3.4$ eV with dispersion $\sigma_B = 0.1$ eV. (a) Number density of polarons and bipolarons. (b) Chemical capacitance of polarons, C_μ^P, bipolarons, C_μ^B, and total capacitance, as a function of Fermi level.

of carriers in sites that is achieved by Bs in comparison to Ps. The capacitance makes two consecutive peaks related to P and B formation, and a third one that is caused by the large negative capacitance of Ps in the high oxidation region. It should also be pointed out that the relative stability of one bipolaron vs. two polarons may depend on the experimental conditions such as solvent and type of counterions [10].

3. Carrier transport

The transport properties of conducting polymers are highly dependent upon the structural disorder arising from sample quality, doping procedure, and aging. Conducting polymers generally display a rich variety in their morphology, being partially crystalline and partially disordered. All the electroactive polymers such as polypyrrole, polythiophene, polyaniline, poly(*p*-phenylene), etc. show an extended localization in their polymer backbone, but disorder and one-dimensionality lead to localization of the electron wave function. Even if the polymer chains are well-ordered, localization occurs in the disordered regions. Polarons move within the aggregates consisting of parallel chains, which probably leads to the formation of metallic islands. Since such domains may be considered as a large-scale clusters of chains, charge transfer between them to avoid the chain break and defects seems to dominate the macroscopic conductivity of the polymer [30].

3.1. Mobility and diffusion coefficient

In the electron transport in metals or band semiconductors, a single transport level consisting of extended states is well defined. Both the mobility u and the diffusion coefficient D are constant, and they satisfy the standard Einstein relation

$$u = \frac{e}{k_B T} D \tag{23}$$

In systems in which the transport is governed by hopping between localized states, the situation is very different. The rate of jumps between near sites (determining the diffusion coefficient) depend critically on the distance, occupation, and energy difference between the sites. These factors may vary widely due to disorder, and change with the position of the Fermi level, which determines the average occupancies of energy levels. It is also important to distinguish random walk displacement of single carriers from the collective transport induced by macroscopic gradient. A formalism recently presented [34] to determine the electronic transport coefficients from electrochemical measurements, based on the formulation of Reed and Ehrlich [39], is briefly outlined in the following, see Ref. [34] for details.

The random walks of an electronic carrier determine the jump diffusion coefficient, that has the form

$$D_J = \frac{1}{6t} \left\langle \left(\frac{1}{N} \sum_{i=1}^{N} \Delta r_i \right)^2 \right\rangle \tag{24}$$

where Δr_i is the displacement of the ith particle at time t, and $\langle\rangle$ denotes a statistical average. D_J can often be expressed, in three-dimensions, as

$$D_J = \frac{1}{6} \langle v \rangle \langle r^2 \rangle \tag{25}$$

in terms of a mean effective jump frequency $\langle v \rangle$, and the square of effective jump length $\langle r^2 \rangle$ [39,40]. On another hand, experimental information on the fundamental jump rates is often derived from the chemical diffusion coefficient, D_p, that relates the flux J to the gradient of the concentration

$$J_p = -D_p \frac{\partial p}{\partial x} \tag{26}$$

Routine electrochemical methods, based on a step of the voltage (either in time or frequency domain), measure the chemical diffusion coefficient, see, e.g. Refs. [41,42]. The diffusion coefficients D_p and D_J differ by the thermodynamic factor, χ_p,

$$D_p = \chi_p D_J \tag{27}$$

$$\chi_p = \frac{p}{k_B T} \frac{\partial \mu}{\partial p} \tag{28}$$

which can be expressed with respect to the chemical capacitance as

$$\chi_p = \frac{e^2 p}{k_B T} \frac{1}{C_\mu} \tag{29}$$

The mobility, appearing in the conductivity, Eq. (1), is proportional to the jump diffusion coefficient

$$u_p = \frac{e D_J}{k_B T} \tag{30}$$

The generalized Einstein relation has the form [34]

$$u_p = \frac{e D_p}{k_B T \chi_p} \tag{31}$$

The conductivity in Eq. (1) can be expressed as

$$\sigma = e^2 D_p \frac{dp}{d\mu} \tag{32}$$

The conductivity can also be written [43]

$$\sigma = D_p C_\mu \tag{33}$$

The significance of Eq. (33) is that all three quantities contained (conductivity, chemical diffusion coefficient, and chemical capacitance) are separately measurable with electrochemical methods.

In summary, the mobility and the chemical diffusion coefficient have different dependencies on the electrochemical potential, since they differ by the thermodynamic factor. The mobility, u_p, is determined from the conductivity and the total carrier density, while the chemical diffusion

coefficient, D_p, is directly measured by transient methods such as EIS. D_p can be also measured indirectly via Eq. (33). It should be further remarked that the electrochemical measurement of chemical diffusion coefficient of electronic carriers by EIS needs special precautions, since the diffusion coefficient of ions is preferentially observed when the polymer is oxidized [3,44].

3.2. Single level model

Let us discuss the application of these concepts with a very simple example without energy disorder [45], that already shows some features observed in conducting polymers. Carrier density and capacitance of a single energy level ε_P, have been discussed in Fig. 2a. We consider the transport of holes by hopping between the neighbor localized sites. The mean effective jump frequency is

$$\langle v\rangle = v_0(1-f_P) \tag{34}$$

where v_0 is the rate constant for hole hopping from an occupied site to an empty site at the distance $R=(N_s)^{-1/3}$ [46]. Eq. (34) accounts for the fact that hopping probability decreases when neighbor sites become occupied. Therefore jump diffusion coefficient is

$$D_J = \frac{\langle v\rangle}{N_s^{2/3}} \tag{35}$$

and the mobility has the form

$$u_p(\eta) = \frac{ev_0}{k_B T N_s^{2/3}}(1-f_P) \tag{36}$$

Since the thermodynamic factor is $\chi_p = 1(1-f_P)$, the chemical diffusion coefficient is a constant, $D_p = v_0R^2$, as explained in Ref. [39], see Fig. 2c. Therefore the conductivity, given by Eq. (33), follows the shape of the chemical capacitance. The peak of the conductivity, shown in Fig. 2b, can be explained by the combined behaviors of carrier density and mobility. As the Fermi level increases the density of holes increases until it reaches a constant level. But then, the mobility starts to decrease because most of the states have been filled.

This simple model shows that there is a correlation of mobility and chemical capacitance, and also the important feature of the saturation and decrease of the conductivity usually observed in experiments, as discussed in the Introduction. However, since the transport in organic conductors usually occurs through hops among localized states characterized by a Gaussian distribution of site energies [36], one should expect a more complex behavior of the transport coefficients as a function of electrochemical potential.

3.3. Gaussian disorder model

Transport in organic materials with a broad density of states is described in terms of a hopping-percolation framework [12,38,47,48]. Instead of hopping between sites with a unique energy level, as in the former example, the transport occurs by carrier jumps via localized states randomly distributed in space and distributed in energy as indicated in Eq. (10). The aim of the models is to calculate the mean effective jump frequency and jump distance, which allow one to find the jump diffusion coefficient via Eq. (25), and consequently the carrier mobility by Eq. (30). However, the disorder both in distance and energy space introduces a very wide set of possible transitions between localized states. Averaging over these configurations is usually very difficult and leads to complicated analytical expressions.

In systems in which the DOS decreases rapidly with the energy, the problem is considerably reduced by the concept of transport energy [12,49,50]. In equilibrium conditions, carriers jump from deep sites, where they are localized, to shallower sites. For carriers situated deep enough energetically, carriers most probably jump from the deep sites to a hopping site that belongs to the transport energy of the level E_{tr}. The occurrence of the effective transport level effectively reduces the hopping transport to multiple trapping, with E_{tr} playing the role of the mobility edge [51], provided that the Fermi level is well below the transport level.

Here we discuss, the model formulated by Arkhipov et al. [52] that includes high carrier density effects. The equation for the energy E_{tr} is

$$\int_{-\infty}^{E_{tr}} \frac{g(E)(E_{tr}-E)^3}{1+\exp[-(E-E_F)/kT]}\mathrm{d}E = \frac{6}{\pi}\left(\frac{kT}{a}\right)^3 \tag{37}$$

where a is the localization length. The average carrier jump rate $\langle v\rangle$ is

$$\langle v\rangle = \frac{v_0}{n}\int_{-\infty}^{E_{tr}} \frac{g(E)}{1+\exp[(E-E_F)/kT]} \times \exp\left(-\frac{E_{tr}-E}{k_BT}\right)\mathrm{d}E \tag{38}$$

The average square jump distance, $\langle r^2\rangle$, is found as

$$\langle r^2\rangle = \left[\int_{E_{tr}}^{\infty} g(E)\mathrm{d}E\right]^{-2/3} \tag{39}$$

We refer to Ref. [52] for the physical origin of these expressions. It has been pointed out [53] that the jump frequency in Eq. (38) should include the tunneling term $\exp(-2r/a)$, however here we maintain the original formulation of the model [52]. The equilibrium mobility is calculated with Eqs. (25) and (30)

$$u_p = \frac{e\langle v\rangle\langle r^2\rangle}{kT} \tag{40}$$

The results of this model for a Gaussian distribution are shown in Fig. 3. Fig. 3a shows the transport energy, which has the value 0.1 eV above the center of the DOS at low carrier densities, and then shifts to higher energies as discussed in Ref. [52]. The conductivity traces a broad peak,

Fig. 3c. At low carrier densities the mobility, shown in Fig. 3d, exhibits a constant value, that is given approximately by the formula [48]

$$u_p = \frac{ev_0}{k_B T N_t^{2/3}} \exp\left[-\frac{E_{tr}}{k_B T} - \frac{E_m}{2k_B T}\right] \quad (41)$$

When the Fermi level increases, the mobility shows an increase because of the decreased distance between the Fermi level and the transport energy, that facilitates thermally activated hops. This is a common feature in multiple trapping models [45]. When the carrier density becomes very high in Fig. 3d, the mobility declines. This is due to the increasing localization of carriers due to the occupation of the DOS, that reduces the number of sites available for hopping. The effect is the same as that found in the simple model of Fig. 2c. However, when the Fermi level is above the center of the DOS the model of Eqs. (38)–(40) is not reliable, because the transport energy concept is not valid at such high carrier densities [52].

The increase of the mobility depends strongly on the disorder parameter σ_P. This is shown in the mobility variation with respect to carrier density presented in Fig. 6 for several σ_P values. The increase of the mobility is even larger if the DOS is a bimodal Gaussian, associated to more and less ordered regions, as described in Ref. [52]. Another effect that causes an increase of the mobility over several orders of magnitude is the presence of traps, that is also described by a bimodal Gaussian [54,55]. Shimotani et al. [28] observed that the hole mobility in poly(3-hexylthiophene) (P3HT) polymer films exhibits a sharp increase under electrochemical doping, while in a field-effect transistor measurement of the same material, the mobility shows a much weaker dependence with the concentration. This effect is attributed to the fact that the counterions in electrochemical charging create deep coulombic traps that broaden the Gaussian DOS. Further developments of the Arkhipov model [56,57] explain the initial mobility decrease observed in some electrochemical measurements [58] in terms of deep Coulomb traps created by doping.

The transport model indicated so far has some limitations for the quantitative interpretation of the electrochemical experiments. The model of Fig. 2 neglects the energy disorder, while the Arkhipov model of in Fig. 3 does not adequately cover the region of decreasing conductivity at high oxidation potentials, although the mobility decrease at high carrier densities has been treated using a more advanced approach [59]. In addition, these models are restricted to a single kind of carrier and neglect the combined transport of P and B species. However, these models already provide a broad view of the features expected in the conductivity, CV and diffusion coefficient during electrochemical oxidation of conducting polymers.

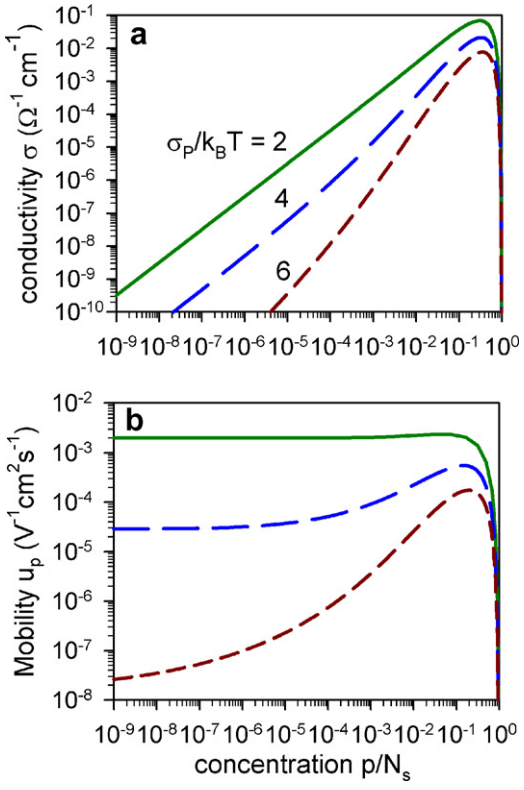

Fig. 6. (a) Conductivity and (b) mobility, calculated according to the transport energy concept, as a function of fractional occupancy of a Gaussian DOS, for different values of the width of the distribution as indicated. The following set of parameters was used in the calculation: $N_s = 1.0 \times 10^{21}$ cm^{-3}, $T = 300$ K, $v_0 = 10^{13}$ s^{-1}, $a = 2 \times 10^{-8}$ cm.

4. Experimental

4.1. General

All electrochemical and spectroelectrochemical experiments described in this work were performed in three electrodes cell. An indium doped tin oxide (ITO) electrode (Delta-technologies, resistivity: 6–12 Ω) was used as a working electrode, an $Ag/AgNO_3$ electrode as a reference electrode and a Pt ribbon as a counter electrode. All experiments performed in Ar glove box atmosphere (H_2O and O_2 <1 ppm). For electrochemistry we used Echo Chemie Autolab PGSTAT20 and PGSTAT30 (with bipot mode) potentiostates.

4.2. Polymerization and Cyclic voltammetry characterization

The polymer di-Cbz-PFP was deposited on the ITO electrode by using cyclic voltammetry method. The polymerization solution contained 10 mM of the monomer in highly grade 1:4 (v:v) dichloromethane–acetonitrile (DCM:AN) solution and 0.16 M of tetrabutylammonium perchlorate ($TBAClO_4$) as a supporting electrolyte. For polymerization we scanned the system four times between 0 and 1.4 V at 50 mV/s, while increasing current from one scan to another indicates the polymer growth. After polymerization the working electrode has been washed

intensively with clean AN to remove monomer leftovers and dipped in clean dry solution of 0.2 M $TBAClO_4$ in AN for the rest of the experiments.

4.3. In situ conductivity experiments

For in situ conductivity experiments we manipulated the working electrode before the polymer deposition in the following way: We created a non-conducting gap (3 μm width) in the middle of the ITO working electrode all along its length and by that we divided it to two individual ITO electrodes (WE1 and WE2). To create the gap we ablated a strip of ITO from the glass by using 355 nm ND:YAG laser beam (JDSU, USA), focused by optic microscope (Olympus AX70, magnification X60). We moved the electrode slowly with an electric motor under the laser beam to control the gap length. We washed the electrode from ITO residues and measured the resistance from one side to another. The measured resistance between WE1 and WE2 is always higher than 200 MΩ, indicating the quality of the gap.

To cover the ITO electrodes and the gap with the polymer, we then shortcut both sides of the electrode with a metal wire and performed the polymerization process described above. We examine the electrode by high resolution scanning electron microscope to ensure the polymer covers both sides of the working electrode and the gap between it.

Measuring of in situ conductivity was done by supplying constant potential to one side of the working electrode (WE2) and increasing potential steps to the other side of it (WE1), i.e. $E_{WE1} = V_1 + \Delta V$; $\Delta V = 0, 5, 10, 15$ mV; $E_{WE2} = V_1$ [5]. We change from one step to another (on WE1) when we identify that the current on both electrodes changes very slowly (typically after 400 s). The current changes on WE2 (ΔI_{WE2}) recorded at different ΔVs, originates from the current coming from WE1 through the polymer on the non-conducting gap. Plotting ΔI_{WE2} vs. ΔV gives $1/R$ (R is resistance) which is proportional to the conductivity.

4.4. Spectroelectrochemistry

Spectra were taken by UV–vis–NIR CARY500 (Varian) spectrometer. Before starting the experiment we held the polymer at −0.5 V for 30 min to ensure its neutral state. To take a spectrum of the polymer at a specific potential (e.g. V_1') we linearly scan the polymer to V_1' and held it at V_1' until we recognize that the current is relatively constant (normally after 20–60 s). Then, we operated the spectrometer and took an absorption spectrum at 350–1600 nm. We assume that the absorbance of the polymer does not change meaningfully during collecting the spectrum (ca. 1 min). When collecting was over, we linearly scanned the polymer back to −0.5 V and held it there for 60 s. We then performed two scans of CV between 0 V and V_1', to monitor the polymer condition (whether it is still active or degraded by over oxidation, etc.). We repeated these steps to take spectra at potentials between 0.3 and 1.6 V at 50 mV steps.

5. Results and discussion

The capacitive nature of the CV of conducting polymers at sufficiently slow scan rates was already demonstrated in Ref. [2] and has been further elaborated in terms of the concept of the chemical capacitance, which is common to many systems [15]. The capacitive response requires that the voltage scan is slow enough for the film to reach equilibrium at each state of charging. Fig. 7a shows the CV of a di-Cbz-PFP film with thickness $L = 1.2$ μm and area 0.77 cm^2 at different scan rates. Using Eq. (4), the CV currents are converted to a capacitance as shown in Fig. 7b. It is observed that the peak heights and positions at the slowest scan rates coincide well, so it can be concluded that the film is in quasi-equilibrium conditions at these slow scan rates and the CV current represents the chemical capacitance of the polymer film.

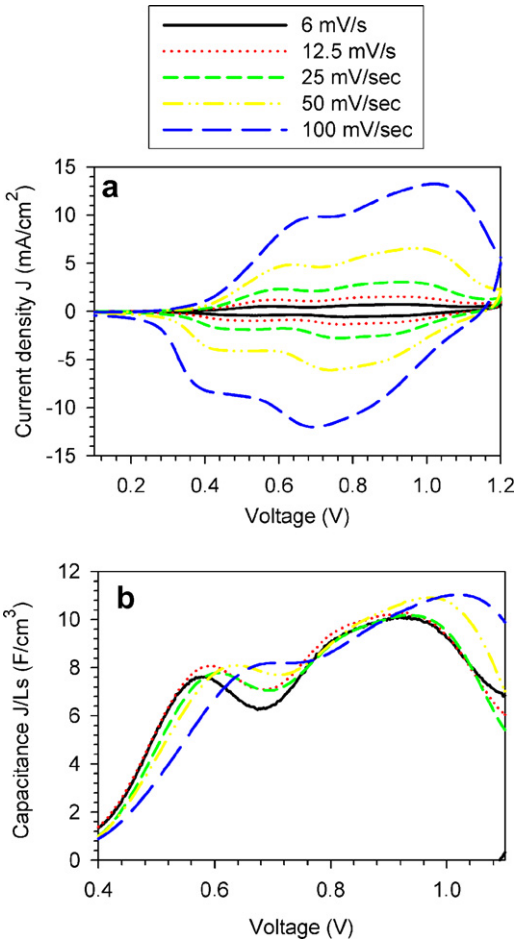

Fig. 7. (a) Cyclic voltammetry of di-Cbz-PFP film at different scan rates s as indicated. (b) Representation of the capacitance per unit volume.

In the absorption spectra, shown in Fig. 8, two absorption bands are developed with increasing potential, at 405 and 801 nm, followed by a third peak appearing in higher potentials (>0.8 V) and located between the former two, at 668 nm. At higher potentials, the later peak increases while the former peaks decrease. This trend does not change up to the highest potential used in this study (Fig. 9a). We relate this spectral behavior to the creation of polarons (P, 405 and 801 nm) and bipolarons (B, 668 nm) [10]. The π–π^* transition of the neutral polymer appears in higher energies ($\lambda < 350$ nm) and is therefore out of our spectral window.

Fig. 9 compares the different results obtained, as a function of the potential. Fig. 9a shows the number of P and B inferred from the absorption spectra. By taking the derivative of Fig. 9a with respect to the potential, the chemical capacitance of the separate P and B species is calculated, Eq. (3), and is shown in Fig. 9b. The chemical capacitance from CV data, Fig. 9c, cannot be separated into the P and B components, but two well-separated peaks are observed. Note that the separate peaks for P and B species are predicted in the model of Fig. 5. Also the negative capacitance feature of P species indicated in Fig. 5 is observed in Fig. 9b. Finally the conductivity is shown in Fig. 9d. σ displays the general features that are known from the literature and were discussed above: A region of increase at increasingly positive potentials and then a decrease at very high oxidation levels. In general the conductivity shows a correlation with the capacitance of the film, and in fact the first CV peak, interpreted as the maximum of P capacitance, is accompanied by a local increase on the conductivity, while the major increase of σ seems to be associated with the B species. The decrease of the conductivity at the more positive potentials is interpreted in terms of saturation of empty hopping sites, as discussed in Section 3.

It is observed that there is a very good correlation of the peak locations in the three experimentally independent curves (b), (c) and (d) of Fig. 9. This result strongly indicates that both P and B species separately respond in the three measurements. Especially the peaks in the spectroelectrochemical capacitance (b) and the conductivity (d) correlate very precisely. On another hand the CV capacitance appears to be positively displaced about 100 mV. This can be understood taking into account the different conditions of the experiments, in which the spectra, the CV, and the conductivity, where taken. As explained in Section 4, the spectroelectrochemistry was done by doping the polymer to a given potential and after taking the spectrum it was de-doped to (−0.5 V) and it was held there for few tens of seconds. These conditions are kinetically much better than cycling a fresh polymer two times at different scan rates. Indeed it is observed in Fig. 7b that the positions of the capacitance peaks are not completely stabilized at the slowest scan rates used. Moreover, considering the lowest potential peak, the polymer was not yet doped to high, damaging potentials (above 1.2 V, which can be seen from the cycling efficiency, not shown) as it is in the CV experiment. It is not surprising, then, that the CV experiment presents worse doping kinetics than the spectroscopy experiment. In terms of electrochemistry conditions, the conductivity experiment resembles the spectroelectrochemistry, rather than CV measurements. In this experiment also, the polymer is still fresh (it has not been continuously scanned to high potentials), and the experiment is done under steady state conditions (see Section 4), but the material has not been de-doped to low potentials.

Using Eq. (33) we can calculate the chemical diffusion coefficient D_P simply dividing the conductivity by the chemical capacitance. The results are displayed in Fig. 10b. It is observed that the general shape of the diffusion coeffi-

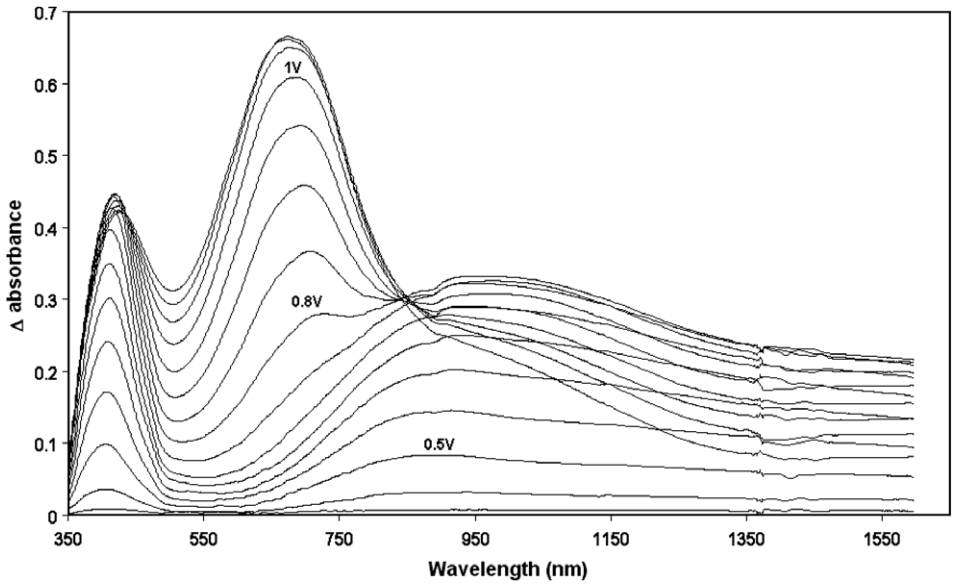

Fig. 8. Absorption spectra of di-Cbz-PFP film at different potentials.

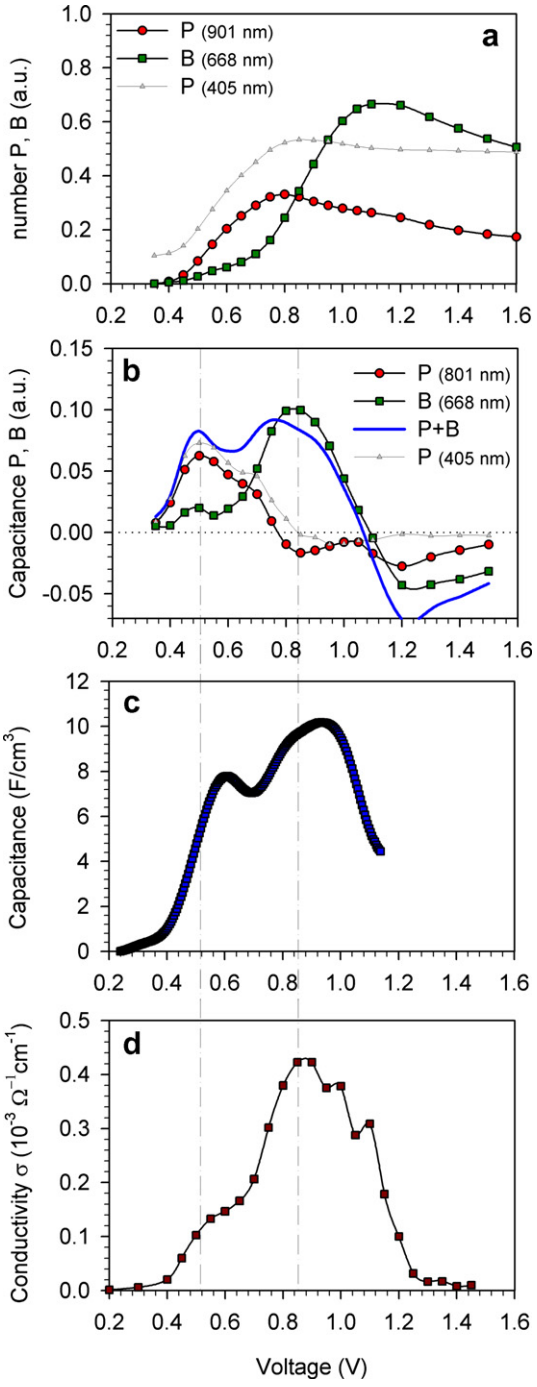

Fig. 9. Experimental results of di-Cbz-PFP film as a function of voltage. (a) Absorption. (b) Derivatives of absorption. (c) Capacitance $s = 25$ mV/s. (d) Conductivity.

cient shows a constant domain at low oxidation levels, followed by and increase and later a decrease at higher carrier densities. Following the model of Fig. 3b, the general variation of D_p observed in Fig. 10b can be interpreted in terms of dominant transport of B, while the small peak near 0.5 V can be attributed to the transport of P. However, we suggest that more work is needed to clearly identify separately the diffusion coefficients of P and B species.

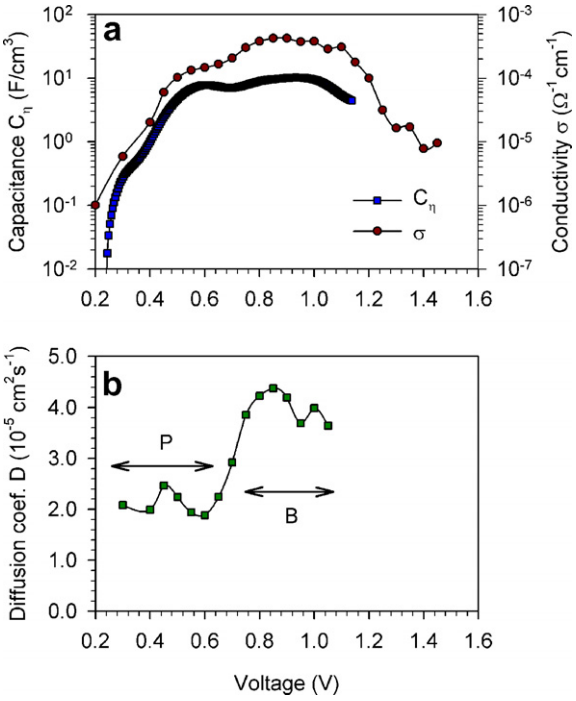

Fig. 10. Experimental results of di-Cbz-PFP film. (a) Capacitance at $s = 25$ mV/s and conductivity in log-linear scale. (b) Diffusion coefficient obtained from $D = \sigma/C_\mu$. The arrows mark the regions attributed to polarons and bipolarons.

6. Conclusion

The electrochemical charging and transport properties of conducting polymers have been described assuming a set of characteristic features of these materials. (i) The formation of polaron and bipolaron species. (ii) The disorder broadening of the energy levels of the separate species. The capacitance may shows different shapes according to the formation energies of the separate species, that determine their relative stability. Carrier transport consists the jumps between a set of localized sites that show disorder both in energy and spatial coordinates, and are furthermore modified by the Coulomb interactions induced by dopant counterions. Therefore, detailed transport features require a very complex description. However, some available models describe important features of the characteristic behavior. Importantly, the correlation between the capacitance and the conductivity indicates that the peaks of both quantities should occur approximately at the same potentials, and this has been confirmed in the di-Cbz-PFP polymer used in this study. The decrease of the mobility at high carrier densities is explained by the exhaustion of empty sites for hopping.

Acknowledgements

The work was supported by Ministerio de Educación y Ciencia of Spain under Projects MAT2004-05168 and HOPE CSD2007-00007 (Consolider-Ingenio 2010) and by

the VIth Framework European project NACBO (Grant NMP3-2004-500802-2).

References

[1] J. Tang, R.D. Allendoerfer, R.A. Osteryoung, J. Phys. Chem. 96 (1992) 3531.
[2] M.D. Levi, C. Lopez, E. Vieil, M.A. Vorotyntsev, Electrochim. Acta 42 (1997) 757.
[3] G. Garcia-Belmonte, J. Bisquert, E.C. Pereira, F. Fabregat-Santiago, J. Electroanal. Chem. 508 (2001) 48.
[4] G. Garcia-Belmonte, J. Bisquert, Electrochim. Acta 47 (2002) 4263.
[5] E.W. Paul, A.J. Ricco, M.S. Wrighton, J. Phys. Chem. 89 (1985) 1441.
[6] F. Genoud, M. Guglielmi, M. Nechtschein, Phys. Rev. Lett. 55 (1985) 118.
[7] G. Paasch, P.H. Nguyen, A.J. Fischer, Chem. Phys. 227 (1998) 219.
[8] J.L. Brédas, G.B. Street, Acc. Chem. Res. 18 (1985) 309.
[9] H. Reiss, J. Phys. Chem. 89 (1985) 3783.
[10] J.A.E.H. van Haare, E.E. Havinga, J.L.J. van Dongen, R.A.J. Janssen, J. Cornil, J.-L. Brédas, Chem. Eur. J. 4 (1998) 1509.
[11] J. Bisquert, G. Garcia-Belmonte, J. García-Cañadas, J. Chem. Phys. 120 (2004) 6726.
[12] S.D. Baranovskii, H. Cordes, F. Hensel, G. Leising, Phys. Rev. B 62 (2000) 7934.
[13] I.N. Hulea, H.B. Brom, A.J. Houtepen, D. Vanmaekelbergh, J.J. Kelly, E.A. Meulenkamp, Phys. Rev. Lett. 93 (2004) 166601.
[14] J. García-Cañadas, F. Fabregat-Santiago, H. Bolink, E. Palomares, G. Garcia-Belmonte, J. Bisquert, Synthetic Met. 156 (2006) 944.
[15] J. Bisquert, F. Fabregat-Santiago, I. Mora-Seró, G. Garcia-Belmonte, E.M. Barea, E. Palomares, Inorg. Chim. Acta (2007), doi:10.1016/j.ica.2007.05.032.
[16] T. Ohsawa, T. Kabata, O. Kimura, M. Onoda, K. Yoshino, Jpn. J. Appl. Phys. 28 (1989) 996.
[17] D. Ofer, R.M. Crooks, M.S. Wrighton, J. Am. Chem. Soc. 112 (1990) 7869.
[18] R. Patil, Y. Harima, K. Yamashita, K. Komaguchi, Y. Itagaki, M. Shiotani, J. Electroanal. Chem. 518 (2002) 13.
[19] R. Patil, Y. Harima, X. Jiang, Electrochim. Acta 49 (2004) 4687.
[20] M. Skompska, J. Mieczkowski, R. Holze, J. Heinze, J. Electroanal. Chem. 577 (2005) 9.
[21] G. Zotti, Synthetic Met. 97 (1998) 267.
[22] G. Zotti, S. Zecchin, B. Vercelli, A. Berlin, S. Grimoldi, M.C. Pasini, M.M.M. Raposo, Chem. Mater. 17 (2005) 6492.
[23] Y. Harima, D.-H. Kim, Y. Tsutitori, X. Jiang, R. Patil, Y. Ooyama, J. Ohshita, A. Kunai, Chem. Phys. Lett. 420 (2006) 387–390.
[24] Y. Harima, F. Ogawa, R. Patil, X. Jiang, Electrochim. Acta 52 (2007) 3615.
[25] H.J. Snaith, M. Grätzel, Phys. Rev. Lett. 98 (2007) 177402.
[26] Q. Zhou, L. Zhuang, J. Lu, Electrochem. Commun. 4 (2003) 733–736.
[27] X.-L. Wei, A.J. Epstein, Synthetic Met. 84 (1997) 791.
[28] H. Shimotani, G. Diguet, Y. Iwasa, Appl. Phys. Lett. 86 (2005) 022104.
[29] P.W.M. Blom, M.C.J.M. Vissenberg, Mater. Sci. Eng. R 27 (2000) 53.
[30] R.S. Kohlman, A.J. Epstein, in: T.A. Skotheim, R.L. Elsenbaumer, J.R. Reynolds (Eds.), Handbook of Conducting Polymers, vol. 1, Marcel Dekker, Inc., New York, 1986, p. 85.
[31] Y. Diamant, E. Furmanovich, A. Landau, J.-P. Lellouche, A. Zaban, Electrochim. Acta 48 (2003) 507.
[32] Z. Pomerantz, G. Garcia-Belmonte, A. Joseph, J.-P. Lellouche, J. Bisquert, A. Zaban, Electrochim. Acta 52 (2007) 6841.
[33] J.C. Scott, P. Pfluger, M.T. Krounbi, G.B. Street, Phys. Rev. B 28 (1983) 2140.
[34] J. Bisquert, Phys. Chem. Chem. Phys. (2007), doi:10.1039/b709316k.
[35] C.E.D. Chidsey, R.W. Murray, J. Phys. Chem. 90 (1986) 1479.
[36] H. Bässler, Phys. Stat. Sol. (b) 175 (1993) 15.
[37] V.I. Arkhipov, P. Heremans, E.V. Emelianova, G.J. Adriaenssens, Appl. Phys. Lett. 79 (2001) 4154.
[38] R. Coehoorn, W.F. Pasveer, P.A. Bobbert, C.J. Michels, Phys. Rev. B 72 (2005) 155206.
[39] D.A. Reed, G. Ehrlich, Surf. Sci. 102 (1981) 588.
[40] A.V. Myshlyatsev, A.A. Stepanov, C. Uebing, V.P. Zhdanov, Phys. Rev. B 52 (1995) 5977.
[41] M.D. Levi, E. Markevich, D. Aurbach, Electrochim. Acta 51 (2005) 98.
[42] C.A. Niklasson, C.-G. Granqvist, J. Mater. Chem. 17 (2007) 127.
[43] J. Bisquert, V.S. Vikhrenko, J. Phys. Chem. B 108 (2004) 2313.
[44] G. Garcia-Belmonte, J. Bisquert, G. Popkirov, Appl. Phys. Lett. 83 (2003) 2178.
[45] J. Bisquert, J. Phys. Chem. B 108 (2004) 2323.
[46] A. Miller, S. Abrahams, Phys. Rev. 120 (1960) 745.
[47] S.D. Baranovskii, I.P. Zvyagin, H. Cordes, S. Yamashi, P. Thomas, Phys. Stat. Sol. (b) 230 (2002) 281.
[48] V.I. Arkhipov, E.V. Emelianova, G.J. Adriaenssens, Phys. Rev. B 64 (2001) 125125.
[49] S.D. Baranovskii, T. Faber, F. Hensel, P. Thomas, J. Phys.: Conden. Mat. 9 (1997) 2699.
[50] O. Rubel, S.D. Baranovskii, P. Thomas, Phys. Rev. B 69 (2004) 014206.
[51] V.I. Arkhipov, P. Heremans, E.V. Emelianova, G.J. Adriaenssens, H. Bässler, Chem. Phys. 288 (2003) 51.
[52] V.I. Arkhipov, P. Heremans, E.V. Emelianova, G.J. Adriaenssens, H. Bässler, Appl. Phys. Lett. 82 (2003) 3245.
[53] S.D. Baranovskii, O. Rubel, P. Thomas, Thin Solid Films 487 (2005) 2.
[54] V.I. Arkhipov, J. Reynaert, Y.D. Jin, P. Heremans, E.V. Emelianova, G.J. Adriaenssens, H. Bässler, Synthetic Met. 138 (2003) 209.
[55] R. Coehoorn, Phys. Rev. B 75 (2007) 155203.
[56] V.I. Arkhipov, E.V. Emelianova, P. Heremans, H. Bässler, Phys. Rev. B 72 (2005) 235202.
[57] V.I. Arkhipov, P. Heremans, E.V. Emelianova, H. Bässler, Phys. Rev. B 72 (2005) 045214.
[58] F. Laquai, G. Wegner, H. Bässler, Philos. Trans. Roy. Soc. A 365 (2007) 1472.
[59] I.I. Fishchuk, V.I. Arkhipov, A. Kadashchuk, P. Heremans, H. Bässler, Phys. Rev. B 76 (2007) 045210.